Microscopy and Microanalysis, **30** (Suppl 1), 2024, 1352–1354
https://doi.org/10.1093/mam/ozae044.666

Microscopy AND Microanalysis

Meeting-report

Corrosion Behavior of New B_4C Ceramic Doped with High-Entropy Alloy in an Aggressive Environment

A.D. Rico-Cano[1], J.C. Mirza-Rosca[1,2,*], B.C. Ocak[3], and G. Goller[3]

[1]*Mechanical Engineering Department, University of Las Palmas de Gran Canaria, Las Palmas de Gran Canaria, Spain*
[2]*Transylvania University of Brasov, Materials Engineering and Welding Department, Brasov, Romania*
[3]*Department of Metallurgical and Materials Engineering, Istanbul Technical University, Maslak, Istanbul, Turkey*

*Corresponding author: julia.mirza@ulpgc.es

Introduction

Boron carbide (B_4C) ceramic shows a unique combination of properties that make it a suitable material for multiple engineering applications, like refractory, electronic or ballistic industry [1]. Eligible properties such as low density, good thermal conductivity and high hardness and melting point makes B_4C an extremely competitive material [2].

High-entropy alloys (HEAs) are a new type of material that contain at least five distinct metallic elements in approximately equal atomic ratio, unlike the traditional metallic alloys, usually composed of one or two main elements [3]. Due to the exceptional properties of HEAs, such as high corrosion resistance, high strength, high ductility and high temperature stability, these materials have gained the scientific community interest [4, 5]. Some potential applications are energy [6, 7], nuclear [8, 9], and biomedical industries [10-12].

Thus, in this study, corrosion properties of new HEA doped B_4C has been investigated to determine its behavior in artificial sea water.

Experimental

Investigations were conducted on B_4C with 2 vol.% CoCrFeNiMo HEA addition, from now on doped sample. This new material was produced by the Metallurgical and Materials Engineering Department of Istanbul Technical University, using spark plasma sintering (SPS) technic (SPS-7.40 MK-VII, SPS Syntex Inc).

Before carrying out the electrochemical tests, the doped sample was encapsulated in a two-component epoxy resin to be easily handled. Afterwards, the sample was polished with the Struers TegraPol-11 polisher in two stages: first polishing with silicon carbide abrasive papers with progressively finer grain sizes varying from 240 to 2000 grit and secondly a final polishing with 0.1μm alpha alumina suspension to obtain a mirror finish polishing. The manufacturing process and sample preparation are shown in Fig.1.

After preparing the sample, three electrochemical tests were performed using the potentiostat BioLogic Essential SP-150 (Bio-Logic Science Instruments SAS, Seyssinet-Pariset, France) and an electrochemical cell: Open circuit potential, linear polarization and Electrochemical Impedance Spectroscopy in a 3.5% NaCl artificial sea water. The software used to set the test parameters and analyse the results it is EC - Lab® v-9.55 and aplicable standard ASTM G5-94(2004) was followed. The used conventional electrochemical cell has three electrodes: doped B_4C as working electrode, the platinum electrode as counter electrode, and the saturated calomel electrode as reference electrode.

Using the software “Ecorr vs. Time” approach, the 24 h open circuit potential of the sample was recorded at every 30 s or every time there was a 100 mV change in potential. The data obtained was analysed and plotted as a graph of potential against time, to determine whether the sample’s corrosion potential is stable over time or exhibits a trend toward passivation or corrosion.

Electrochemical Impedance Spectroscopy (EIS) is a nondestructive test that measures electrochemical impedance. It works by applying an alternating current potential to an electrochemical cell while it measures the current through the cell main results. Applicable standard ISO 16773-1-4:2016 was followed.

The "Linear Polarisation" approach was used to carry out these measurements and its potential was stabilised by entering the sample surface area value and the test time of 110 minutes. The potential scanning showed a 10 mV/minute time-variation relationship from - 0.1 to 1 V vs open circuit potential, with data recorded of intensity during the potential variation scanning. After the plotting of these linear polarisation curves, the corrosion rate values of the sample were determined using EC-Lab’s "Tafel Fit" technique.

Results and discussion

Fig. 2 illustrates scanning electron microscope (SEM) images of the surfaces of B_4C and doped B_4C-HEA ceramics that have been etched using electrochemical methods. The monolithic B_4C material exhibits a porous microstructure characterized by a non-uniform distribution of grain size and shape. The B_4C material exhibits the lowest relative density compared to doped ceramic sample. The triangular and uniformly dispersed pores were primarily found at the intersections of three boundaries and the interfaces between grains. Microstructural investigations indicate that the doping led to a more compact microstructure in comparison to the solid B_4C material.

The distribution of doping HEA has been shown to be homogeneous, with the majority positioned on the grain borders and filled pores at several grain junctions inside the B_4C matrix. According to German et al. [13], the liquid phase functions as a substance that fills the pores, rather than spreading over the solid grains, when there is no solubility between the solid and liquid phases. Due to inadequate liquid levels, the samples still retain holes as they were not completely filled. Based on the photos,

Downloaded from https://academic.oup.com/mam/article/30/Supplement_1/ozae044.666/7719738 by Biblioteca ULPGC user on 21 October 2024

the incorporation of HEA phase leads to the removal of voids within the matrix through the process of liquid phase sintering. These tendencies are consistent with the shape of open circuit potential during immersion in artificial sea water (see Fig.3a).

The average grain size of the monolithic B_4C was determined to be 2.57 μm and an uneven distribution of grain sizes was found and was attributed to the rapid heating and melting of impurities that were already present in the initial powders. The doped ceramic yielded a more homogeneous distribution of particle sizes, with the smallest grain size measuring 2.16 μm. These observations suggest that the presence of HEA phases at the grain borders and triple junction locations inhibits grain expansion and results in a finer grain structure. As a result of the tendency of high-entropy alloys to gravitate towards the configuration with the lowest energy, HEA phases predominantly inhabited the smaller grains. It was found [13] that liquid phases have a tendency to occupy the configuration with the lowest energy, leading them to flow preferentially towards smaller grains and pores and in this way explain the linear polarization behavior (see Fig.3b).

The electrochemical impedance spectroscopy data (see Fig.4) showed a very high resistance to corrosion in artificial sea water. Nyquist diagram (Fig.4a) depicts three zones: one semicircle at high frequencies, another semicircle at medium frequencies and a diffusion line at high frequencies. The behavior is characterized by a process in two stages (Fig.4b): first the filling of the pores with sea water (with an important diffusional component) and second the formation of a passive film inside the pores and on the surface of the sample.

Conclusions

The behavior of a high entropy alloy doped B_4C in artificial sea water was studied and the main conclusions are listed as follows:

- The doping of B_4C ceramic with CoCrFeMoNi high entropy alloy led to a more compact microstructure in comparison to the solid B_4C material, inhibits grain expansion and results in a finer grain structure.
- The doped sample has a very high resistance to corrosion in artificial sea water.
- The chemical process which takes place at immersion of the doped sample in artificial sea water has two steps with an important diffusional component.

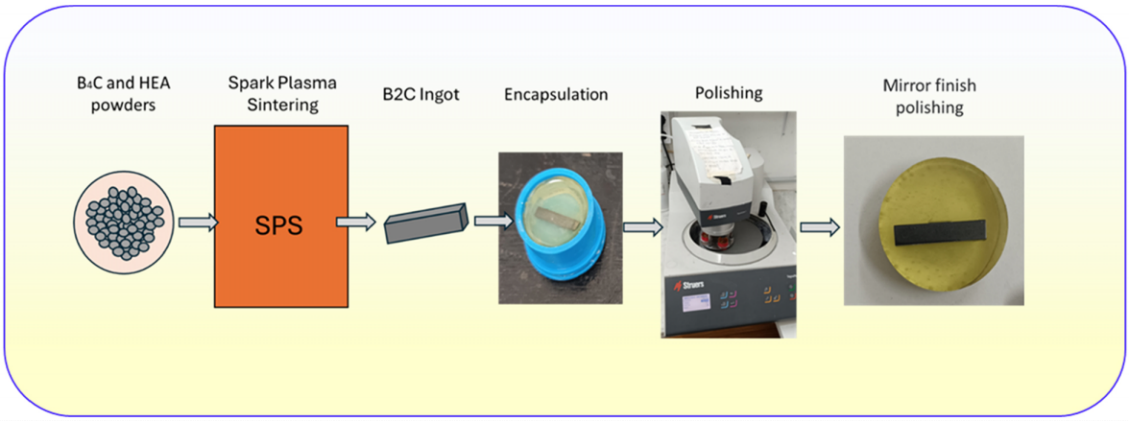

Fig. 1. Sample manufacturing process and preparation.

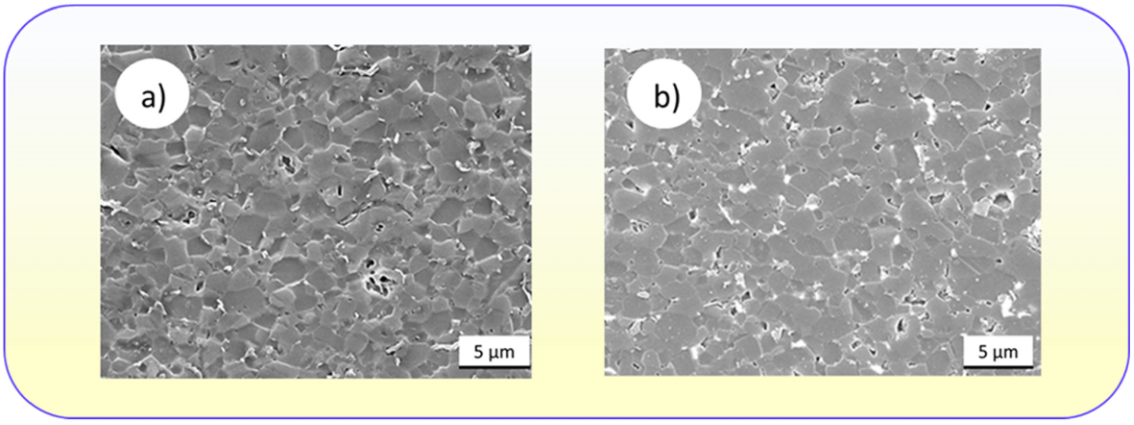

Fig. 2. SEM images of the a) B_4C ceramic and b) HEA doped ceramic.

Downloaded from https://academic.oup.com/mam/article/30/Supplement_1/ozae044.666/7719738 by Biblioteca ULPGC user on 21 October 2024

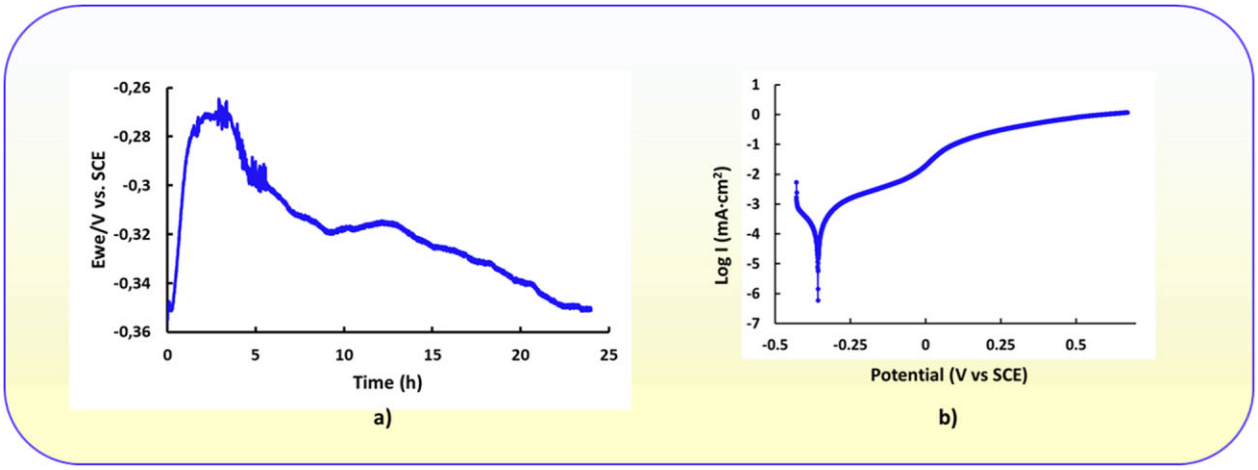

Fig. 3. a) Corrosion potential vs. time for 24 h of immersion and b) Linear polarization in 3.5% NaCl solution.

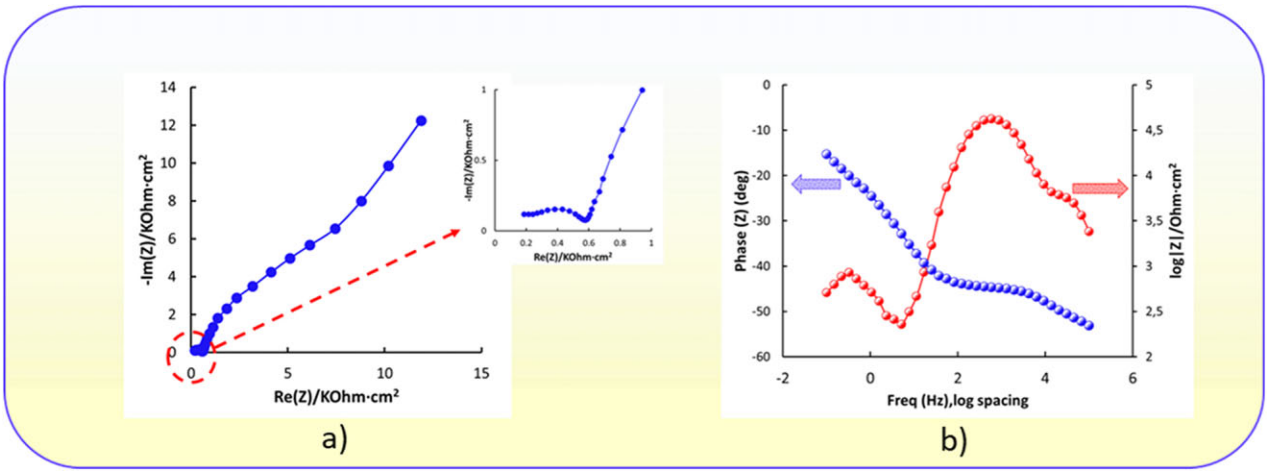

Fig. 4. Impedance diagrams: a) Nyquist; b) Bode-IZI and Bode-phase, for dopped sample in 3.5% NaCl

References

1. V. Domnich *et al.*, *Journal of the American Ceramic Society* **94**(11) (2011), p. 3605–3628. https://doi.org/10.1111/j.1551-2916.2011.04865.x.
2. B. Yavas *et al.*, *Ceram Int* **41**(7) (2015), p. 8936–8944. https://doi.org/10.1016/j.ceramint.2015.03.167.
3. G. Cui *et al.*, *Journal of Materials Research and Technology* **9**(2) (2020), p. 2598–2609. https://doi.org/10.1016/j.jmrt.2019.12.090.
4. S. J. Brito-Garcia *et al.*, *Metals (Basel)* **13**(5) (2023), p. 854. https://doi.org/10.3390/met13050854.
5. S. J. Brito-Garcia *et al.*, *Metals (Basel)* **13**(5) (2023), p. 883. https://doi.org/10.3390/met13050883.
6. F. Yang *et al.*, *International Journal of Hydrogen Energy* **47**(21) (2022), p. 11236–11249. https://doi.org/10.1016/j.ijhydene.2022.01.141.
7. M. Fu et al., *Iscience*, **24**(3) (2021). https://doi.org/10.1016/j.isci.2021.102177
8. M. L. Rios *et al.*, *Microscopy and Microanalysis* **26**(S2) (2020), p. 406–407. https://doi.org/10.1017/s1431927620014555.
9. T. Li *et al.*, *Metals* **13**(2) (2023), p. 363. https://doi.org/10.3390/met13020363.
10. P. Socorro-Perdomo *et al.*, *Microscopy and Microanalysis* **27**(S1) (2021), p. 1772–1774. https://doi.org/10.1017/s1431927621006486.
11. M. López Ríos *et al.*, *Scientific Reports* **10**(1) (2020), p. 21119. https://doi.org/10.1038/s41598-020-78108-5.
12. D. Castro *et al.*, *Metals* **11**(4) (2021), p. 648. https://doi.org/10.3390/met11040648.
13. R.M. German *et al.*, *Journal of materials science* **44** (2009), p. 1-39. https://doi.org/10.1007/s10853-008-3008-0.

Downloaded from https://academic.oup.com/mam/article/30/Supplement_1/ozae044.666/7719738 by Biblioteca ULPGC user on 21 October 2024